Wideband NF-ISAC: Subcarrier Allocation for Sensing and Beamforming

Diluka Galappaththige, *Member, IEEE* and Chintha Tellambura, *Fellow, IEEE*.

***Abstract*—Beamforming for wideband (WB) near-field (NF) integrated sensing and communication (ISAC) systems with multiple users and sensing targets has not yet been fully developed. Moreover, classical optimization methods become computationally expensive in this case. To overcome this challenge, we propose the augmented Lagrangian manifold optimization (MO) for the WB NF-ISAC (ALM-WNI) algorithm, leveraging NF beam-focusing to enhance sum rates and sensing gain while reducing communication-sensing interference. The design includes subcarrier allocation/selection for sensing and beamforming. Non-convex communication-only and joint communication-sensing subcarrier problems are solved using the ALM-WNI framework. By reformulating the problems on a low-dimensional manifold, ALM-WNI reduces the search space from MKL to $(M+1)(K+L)$, where M, L, and L are the number of base station (BS) antennas, users, and targets, respectively, achieving substantial computational savings compared to the convex-concave procedure algorithm (CCPA). For instance, with 257 BS antennas, it achieves a 20-fold speedup over the CCPA, making it well-suited for large-scale, WB NF-ISAC deployments.**

***Index Terms*—Integrated sensing and communication, Near-field, Wideband communication, Subcarrier allocation, Beamforming, Manifold optimization.**

I. Introduction

Near-field (NF) integrated sensing and communication (ISAC) is emerging as a key 6G enabler, leveraging massive antenna arrays and the large bandwidths available from $10\,\mathrm{GHz}$ to $10\,\mathrm{THz}$ [1]–[4]. However, most NF-ISAC beamforming studies focus on narrowband models [5], [6], with wideband (WB) counterparts receiving little attention. One notable exception is [1], which investigates a communications-centric WB NF-ISAC design where communication and sensing (C&S), subcarrier allocation (SA), and beamforming must be jointly optimized. Here, communication beamforming is reused for sensing, but this approach restricts the sensing degrees of freedom (DoF). Due to the NF beam-focusing effect, communication beams concentrate energy into a narrow spatial region, limiting coverage and sensing performance.

To address these limitations, our approach allocates sensing subcarriers while jointly designing beamforming for C&S. Unlike [1], we employ dedicated C&S beamformers, thereby increasing the sensing DoF and enabling more flexible and effective sensing.

The design in [1] relies on successive convex approximation (SCA) for SA and Riemannian manifold optimization (MO) for beamforming. SCA tackles non-convex problems by iteratively solving convex surrogates obtained by linearizing the non-convex components around the current iterate, which tends to sub-optimal solutions [7]. Although MO is used for beamforming, the sensing constraint is enforced through a fixed penalty term, i.e., sub-optimal C&S trade-offs [8].

In contrast, we apply MO to both SA and beamforming. For the beamforming stage, we introduce a new MO framework based on an augmented Lagrangian method (ALM) that offers an adaptive approach tailored to WB NF-ISAC requirements.

We first employ communication-only (CO) beamforming, ignoring the targets. Accordingly, several subcarriers are allocated for sensing. Specifically, each target is sensed by a dedicated subcarrier. Thus, some subcarriers are used for both C&S. For those subcarriers, beamforming is updated to account for both users and targets. These problems are non-convex and NP-hard. Using ALM, we incorporate a penalty term for violations of the beampattern gain (BG) target into the objective function and then minimize the augmented objective over a complex sphere manifold (CSM). We refer to this method as the augmented Lagrangian MO for the WB NF-ISAC (ALM-WNI) algorithm. It iteratively adjusts the optimization variables and the Lagrange and penalty parameters to satisfy all constraints. ALM-WNI has significantly lower computational complexity and runtime than the WB NF-ISAC, even with standard optimization techniques [1]. For instance, with 257 base-station (BS) antennas, ALM-WNI achieves nearly a 20-fold reduction in runtime while maintaining/slightly improving C&S performance compared with the conventional convex-concave procedure (CCPA).

Beyond reducing computational complexity, the proposed ALM-WNI framework improves solution reliability by ensuring exact satisfaction of constraints [8]. It directly optimizes beamformers on the feasible manifold and enforces sensing BG constraints via ALM, driving violations to zero upon convergence [8]. In contrast, CCPA applies semidefinite relaxation (SDR) followed by Gaussian randomization (GR) to recover rank-one solutions; although the relaxed problem satisfies the constraints, the GR step does not guarantee feasibility and may introduce violations [8]. Consequently, ALM-WNI achieves comparable or slightly better sum-rate performance while ensuring feasibility, making it well-suited for large-scale WB NF-ISAC systems in which GR becomes inefficient.

Notation: $\mathbf{I}_M$ is the $M\times M$ identity matrix. $\Re(\cdot)$ denotes the real part. $\mathcal{CN}(\boldsymbol{\mu},\mathbf{R})$ is a complex Gaussian vector with mean $\boldsymbol{\mu}$ and co-variance $\mathbf{R}$. $\mathbf{1}_{\{x\}}$ is 1 if $x>0$ and 0 otherwise. $\mathrm{unt}(\mathbf{a}) = [a_1/|a_1|,\ldots,a_n/|a_n|]$. $\mathbf{A}\circ\mathbf{B}$ is the Hadamard product. $\mathrm{clip}_{[a,b]}(x)=\max\{a,\min(b,x)\}$ is the clip operator.

II. Preliminaries

1) System Model: It includes an $M=2\tilde{M}+1$-antenna BS, K single-antenna users, and L sensing targets (Fig. 1).

D. Galappaththige and C. Tellambura are with the Department of Electrical and Computer Engineering, University of Alberta, Edmonton, AB, T6G 1H9, Canada (e-mail: {diluka.lg, ct4}@ualberta.ca).

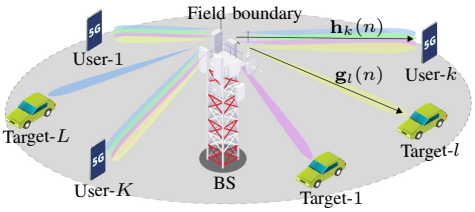

Fig. 1: A WB NF-ISAC system.

The BS simultaneously transmits probing signals to the targets and data signals to users, and employs a uniform linear array (ULA) with an antenna spacing of $d = \lambda_c/2$ and the coordinate system's origin at the center of the ULA, where λ_c denotes the signal wavelength of the center frequency f_c [5], [6]. The ULA aperture is $D = (M-1)d$, with a Rayleigh distance of $2D^2/\lambda_c$ [2]. The users and sensing targets reside in the BS's NF region [5], [6]. Let $\mathcal{N} = \{1, \ldots, N\}$ denote the set of subcarriers and $\mathcal{N}_L$ be a subset of $\mathcal{N}$. In particular, the subcarriers $n \in \mathcal{N}_L$ are designed for joint C&S, whereas the remaining subcarriers $n \in \mathcal{N} \setminus \mathcal{N}_L$ are CO.

2) Channel Model: We use the NF spherical wave channel model [5]. The channels from the BS to the k-th user and the l-th target at the n-subcarrier are denoted by $\mathbf{h}_k(n) \in \mathbb{C}^{M\times 1}$ and $\mathbf{g}_l(n) \in \mathbb{C}^{M\times 1}$, respectively. The NF channel between the BS and the b-th node (user or target) at n-subcarrier is expressed as $\mathbf{f}_b(n) = \beta_b \mathbf{a}_b(n)$, where $b = \{k, l\}$, $\mathbf{f} \in \{\mathbf{h}, \mathbf{g}\}$, $\mathbf{a}_b(n) \in \mathbb{C}^{M\times 1}$ is the NF array response vector with the m-th element $[\mathbf{a}_b(n)]_m = e^{-j\frac{2\pi f_n}{c} r_{mb}(r_b,\theta_b)}$, and $r_{mb}(r_b, \theta_b)$ is the distance from the m-th antenna element to the b-th node and given in [5, Eqn. (1)]. Here, r_b and θ_b are the b-th node distance and angle from the center of the ULA, respectively, $\beta_b = \sqrt{\lambda/4\pi} r_b^{-1}$ is the free-space path-loss between the 0-th antenna and the b-th node. Moreover, $f_n = f_c + B(n-N)/2N$ is the n-th subcarrier frequency, B is the system bandwidth, and c is the speed of light.

3) Transmission Model: Based on the SA, the BS transmits signal $\mathbf{x}(n) \in \mathbb{C}^{M\times 1}$ at the n-th subcarrier, i.e., either for dedicated communication or joint C&S,

$$\mathbf{x}(n) = \begin{cases} \sum_{k=1}^{K} \mathbf{w}_k(n) q_k(n) + \mathbf{s}(n), & \text{for } n \in \mathcal{N}_L, \\ \sum_{k=1}^{K} \mathbf{w}_k(n) q_k(n), & \text{for } n \in \mathcal{N} \setminus \mathcal{N}_L, \end{cases} \tag{1}$$

where $q_k(n) \in \mathbb{C}$ is the unit-power data symbol for the k-th user, i.e., $\mathbb{E}\{|q_k(n)|^2\} = 1$, $\mathbf{w}_k(n) \in \mathbb{C}^{M\times 1}$ is the beamforming vector for the k-th user, and $\mathbf{s}(n) \in \mathbb{C}^{M\times 1}$ is the sensing signal for detecting the assigned target at the $n \in \mathcal{N}_L$-th subcarrier. It is assumed that $q_k(n)$ and $\mathbf{s}(n)$ are independent of each other for $k \in \mathcal{K}$ and $n \in \mathcal{N}_L$ [9]. The received signal at the k-th user at the n-th subcarrier is given as

$$y_k(n) = \begin{cases} \sum_{i=1}^{K} \mathbf{h}_k^{\mathrm{H}}(n) \mathbf{w}_i(n) q_i(n) + \mathbf{h}_k^{\mathrm{H}}(n) \mathbf{s}(n) + z_k(n), \\ \qquad \text{for } n \in \mathcal{N}_L, \\ \sum_{i=1}^{K} \mathbf{h}_k^{\mathrm{H}}(n) \mathbf{w}_i(n) q_i(n) + z_k(n), \\ \qquad \text{for } n \in \mathcal{N} \setminus \mathcal{N}_L, \end{cases} \tag{2}$$

where $z_k(n) \sim \mathcal{CN}(0, \sigma^2)$ denotes the k-th user additive white Gaussian noise (AWGN) at the n-th subcarrier.

The beamforming vectors are organized into single matrices $\mathbf{W}(n) = [\mathbf{w}_1(n), \ldots, \mathbf{w}_K(n)] \in \mathbb{C}^{M\times K}$ for $n \in \mathcal{N} \setminus \mathcal{N}_L$ and $\mathbf{V}(n) = [\mathbf{w}_1(n), \ldots, \mathbf{w}_K(n), \mathbf{s}(n)] \in \mathbb{C}^{M\times(K+1)}$ for $n \in \mathcal{N}_L$. Identity matrices $\mathbf{E} = \mathbf{I}_K \in \mathbb{R}^{K\times K}$ and $\tilde{\mathbf{E}} = \mathbf{I}_{K+1} \in \mathbb{R}^{(K+1)\times(K+1)}$ are defined. The combination of $\{\mathbf{W}(n), \mathbf{V}(n)\}$ and $\{\mathbf{E}, \tilde{\mathbf{E}}\}$ allows the representation of individual columns of $\{\mathbf{W}(n), \mathbf{V}(n)\}$.

III. SA and Beamforming

Here, we discuss the SA for sensing and beamforming. This involves three main steps: (i) CO beamforming, (ii) SA for sensing, and (iii) Refine beamforming for C&S.

1) CO Beamforming: The BS first designs CO beamforming by assuming the absence of sensing targets. For each subcarrier, BS aims to maximize the communication sum rate, and the optimization problem is given as

$$\mathbf{P}_{\mathrm{c}}: \max_{\mathbf{W}(n)} \quad \sum\nolimits_{k=1}^{K} \log_2(1 + \bar{\gamma}_k(n)), \ \forall n, \tag{3a}$$

$$\text{s.t.} \quad \mathrm{Tr}(\mathbf{W}(n)\mathbf{W}^{\mathrm{H}}(n)) \le p_{\max}, \ \forall n, \tag{3b}$$

where (3b) sets the maximum BS transmit power, i.e., $p_{\max}$, and $\bar{\gamma}_k(n)$ is the k-th user SINR, obtained using (2) as

$$\bar{\gamma}_k(n) = \frac{|\mathbf{h}_k^{\mathrm{H}}(n)\mathbf{W}(n)\mathbf{E}_k|^2}{\sum_{i\neq k}^{K} |\mathbf{h}_k^{\mathrm{H}}(n)\mathbf{W}(n)\mathbf{E}_i|^2 + \sigma^2}, \ \forall k, \tag{4}$$

where $\mathbf{E}_k$ is the k-th column of $\mathbf{E}$. Solving $\mathbf{P}_{\mathrm{c}}$ yields the optimal CO beamforming vectors, i.e., $\bar{\mathbf{w}}_k(n)$, for all subcarriers, which are subsequently used for sensing SA.

2) SA for Sensing: The BS uses $\bar{\mathbf{w}}_k(n)$ to allocate sensing subcarriers. Each target is allocated a unique subcarrier, with no subcarrier being shared among targets. However, more general cases can be treated in future work.

The BS computes the transmit BG for each target across subcarriers. BG is a valuable criterion for sensing signal design in ISAC [10]. It represents the transmit power distribution over sensing angles $\theta \in [-\pi/2, \pi/2]$, which enhances detection, range/Doppler/angle estimation, tracking, and sensing accuracy through proper echo signal processing. For the l-th target at the n-th subcarrier, BG is defined as [10]

$$\begin{aligned} \bar{b}_l(n) &= \mathbb{E}\left\{|\mathbf{g}_l^{\mathrm{H}}(n)\mathbf{x}(n)|^2\right\} \\ &= \sum\nolimits_{i=1}^{K} \mathbf{g}_l^{\mathrm{H}}(n)\bar{\mathbf{w}}_i(n)\bar{\mathbf{w}}_i^{\mathrm{H}}(n)\mathbf{g}_l(n), \ \forall l, n. \end{aligned} \tag{5}$$

We impose a constraint that BG must exceed a prescribed threshold to guarantee adequate target illumination [10], as reflected in the basic formulation (6). This formulation can be extended in several directions. First, sidelobe suppression can be enforced through additional angular constraints; however, in the WB-NF regime, this would significantly increase problem dimensionality and computational complexity. The proposed ALM-WNI algorithm can nevertheless accommodate such constraints via additional penalty terms. Second, the model can be refined to explicitly account for the received echo power, incorporating radar cross-section, two-way propagation loss, and receiver processing effects. These extensions are deferred to future work.

Based on the maximum BG, a subcarrier is allocated to each target. For example, let us consider $L = 3$ and $N = 8$. The BGs for all targets at all subcarriers are calculated using the CO beamforming, i.e.,

$[\bar{b}_1(1),\ldots,\bar{b}_1(8);\ldots;\bar{b}_3(1),\ldots,\bar{b}_3(8)]$, resulting in $L\times N=24$ BG values. Among these, the maximum BG value is first selected, and the corresponding target is assigned to the corresponding subcarrier. Then, the respective BG values of the target and the subcarrier are set to zero in the pool of BGs. For example, if the maximum value corresponds to the second target at the seventh subcarrier, set $\bar{b}_2(1)=\cdots=\bar{b}_2(8)=0$ and $\bar{b}_1(7)=\bar{b}_2(7)=\bar{b}_3(7)=0$. The process is repeated until all targets are assigned subcarriers. Let the set of subcarriers assigned for the targets be $\mathcal{N}_L$.

3) Refine Beamforming for C&S: For subcarriers $n\in\mathcal{N}\setminus\mathcal{N}_L$, the CO beamforming obtained in Section III-1 remains optimal. In contrast, for sensing subcarriers $n\in\mathcal{N}_L$, the beamforming must be redesigned to incorporate sensing. Accordingly, the BS jointly optimizes C&S beamforming on $\mathcal{N}_L$ by solving the following problem:

$$\mathbf{P}_{\rm s}:\max_{\mathbf{W}(n)}\quad\sum\nolimits_{k=1}^{K}\log_2(1+\gamma_k(n)),\ \forall n\in\mathcal{N}_L, \tag{6a}$$

$$\text{s.t.}\quad b_{l_n}(n)\geq\Gamma_{\rm th},\ \forall n\in\mathcal{N}_L, \tag{6b}$$

$$\mathrm{Tr}(\mathbf{V}(n)\mathbf{V}^{\rm H}(n))\leq p_{\max},\ \forall n\in\mathcal{N}_L, \tag{6c}$$

where $\bar{\gamma}_k(n)$ is the received SINR at the k-th user at the n-th subcarrier for $n\in\mathcal{N}_L$ and defined as

$$\gamma_k(n)=\frac{|\mathbf{h}_k^{\rm H}(n)\mathbf{V}(n)\tilde{\mathbf{E}}_k|^2}{\sum_{i\neq k}^{K+1}|\mathbf{h}_k^{\rm H}(n)\mathbf{V}(n)\tilde{\mathbf{E}}_i|^2+\sigma^2},\ \forall k, \tag{7}$$

where $\tilde{\mathbf{E}}_k$ is the k-th column of $\tilde{\mathbf{E}}$, (6b) ensures the sensing BG required for the assigned l_n-th target at the $n\in\mathcal{N}_L$-th subcarrier, in which $\Gamma_{\rm th}$ is the intended sensing BG, (6c) indicates the maximum BS transmit power, and $b_{l_n}(n)$ is the BG of the l_n-th target assigned to n-th subcarrier, i.e.,

$$b_{l_n}(n)=\sum\nolimits_{i=1}^{K+1}\mathbf{g}_{l_n}^{\rm H}(n)\mathbf{V}(n)\tilde{\mathbf{E}}_i\tilde{\mathbf{E}}_i^{\rm H}\mathbf{V}^{\rm H}(n)\mathbf{g}_{l_n}(n). \tag{8}$$

By solving $\mathbf{P}_{\rm s}$, the optimal beamforming for both C&S, i.e., $\{\hat{\mathbf{w}}_k(n),\hat{\mathbf{s}}(n)\}$, for the $\mathcal{N}_L$ set of subcarriers are obtained. Thereby, the optimal BS beamforming is assigned as

$$\{\mathbf{w}_k^o(n),\mathbf{s}^o(n)\}=\begin{cases}\hat{\mathbf{w}}_k(n),\hat{\mathbf{s}}(n), & \text{for } n\in\mathcal{N}_L,\\ \bar{\mathbf{w}}_k(n), & \text{for } n\in\mathcal{N}\setminus\mathcal{N}_L.\end{cases} \tag{9}$$

IV. Proposed Solution

This section solves $\mathbf{P}_{\rm c}$ and $\mathbf{P}_{\rm s}$ using fractional programming (FP) and MO to obtain optimal $\mathbf{w}_k^o(n)$ and $\mathbf{s}^o(n)$ [8]. The key challenge is their non-convex objective functions.

1) Solution for $\mathbf{P}_{\rm c}$: To deal with sum-log terms, the FP technique is used to substitute auxiliary variables, $\bar{\boldsymbol{\mu}}(n)=[\bar{\mu}_1(n),\ldots,\bar{\mu}_K(n)]$, for each SINR term in (3a) while ensuring $\bar{\mu}_k(n)\leq\bar{\gamma}_k(n)$. Thus, $\mathbf{P}_{\rm c}$ is equivalently recast as [11]

$$\mathbf{P}_{\rm c1}:\max_{\mathbf{W}(n),\bar{\boldsymbol{\mu}}(n)}f(\mathbf{W}(n),\bar{\boldsymbol{\mu}}(n))=\frac{1}{\ln(2)}\sum\nolimits_{k=1}^{K}\ln(1+\bar{\mu}_k(n))+\frac{1}{\ln(2)}\sum\nolimits_{k=1}^{K}\left(-\bar{\mu}_k(n)+\frac{(1+\bar{\mu}_k(n))\bar{\gamma}_k(n)}{1+\bar{\gamma}_k(n)}\right), \tag{10a}$$

$$\text{s.t.}\quad\text{(3b)}. \tag{10b}$$

$\mathbf{P}_{\rm c1}$ includes two optimization problems: (i) an outer optimization over $\mathbf{W}(n)$ for fixed $\bar{\boldsymbol{\mu}}(n)$ and (ii) an inner optimization over $\bar{\boldsymbol{\mu}}(n)$ for fixed $\mathbf{W}(n)$ [11]. Consequently, $\mathbf{P}_{\rm c1}$ is solved by alternatively optimizing $\mathbf{W}(n)$ and $\bar{\boldsymbol{\mu}}(n)$ until the objective function converges.

Optimizing $\bar{\boldsymbol{\mu}}(n)$: For a given $\mathbf{W}(n)$, $f(\mathbf{W}(n),\bar{\boldsymbol{\mu}}(n))$ is a concave differentiable function of $\bar{\boldsymbol{\mu}}(n)$. Thus, the closed-form optimal $\bar{\boldsymbol{\mu}}(n)$ is obtained by setting each $\frac{\partial f(\mathbf{W}(n),\bar{\boldsymbol{\mu}}(n))}{\partial\mu_k(n)}$ to zero, and optimal $\bar{\mu}_k^o(n)$ is given as $\bar{\mu}_k^o(n)=\bar{\gamma}_k(n)$. Once $\bar{\boldsymbol{\mu}}^o(n)$ is substituted back into $f(\mathbf{W}(n),\bar{\boldsymbol{\mu}}(n))$, the exact sum-of-logarithms objective function in $\mathbf{P}_{\rm c}$ can be recovered.

Optimizing $\mathbf{W}(n)$: For a given $\bar{\boldsymbol{\mu}}(n)$, the objective (10a) can be simplified by eliminating the constant terms with respect to $\mathbf{W}(n)$. Thereby, $\mathbf{P}_{\rm c1}$ is reformulated as

$$\mathbf{P}_{\rm c2}:\max_{\mathbf{W}(n)}\quad\sum\nolimits_{k=1}^{K}\frac{\bar{\mu}_k'(n)|\mathbf{h}_k^{\rm H}(n)\mathbf{W}(n)\mathbf{E}_k|^2}{\sum_{i=1}^{K}|\mathbf{h}_k^{\rm H}(n)\mathbf{W}(n)\mathbf{E}_i|^2+\sigma^2}, \tag{11a}$$

$$\text{s.t.}\quad\text{(3b)}, \tag{11b}$$

where $\bar{\mu}_k'(n)=1+\bar{\mu}_k(n)$. Here, as $\mathbf{P}_{\rm c2}$ retains equivalence with the original problem $\mathbf{P}_{\rm c}$, no performance loss ensues [12].

To solve $\mathbf{P}_{\rm c2}$, we use MO. First, to formulate the manifold, the power constraint is normalized and modified such that $\mathrm{Tr}(\tilde{\mathbf{W}}(n)\tilde{\mathbf{W}}(n)^{\rm H})=\mathrm{Tr}(\mathbf{W}(n)\mathbf{W}(n)^{\rm H}+\|\boldsymbol{\vartheta}(n)\|_2^2=1$, where $\tilde{\mathbf{W}}(n)=[\tilde{\mathbf{w}}_1(n),\ldots,\tilde{\mathbf{w}}_K(n)]$, $\tilde{\mathbf{w}}_k(n)=[\mathbf{w}_k(n)^{\rm T},\vartheta_k(n)]^{\rm T}$, and $\boldsymbol{\vartheta}(n)=[\vartheta_1(n),\ldots,\vartheta_K(n)]$ is an auxiliary vector introduced to simplify power normalization while preserving the constraint. This leads to a CSM as $\mathcal{M}_{\rm c}=\{\tilde{\mathbf{W}}(n)\in\mathbb{C}^{(M+1)\times K}\,|\,\mathrm{Tr}(\tilde{\mathbf{W}}(n)\tilde{\mathbf{W}}(n)^{\rm H})=1\}$. As a result, $\mathbf{P}_{\rm c2}$ can be converted into an unconstrained problem on $\mathcal{M}_{\rm c}$ and given as

$$\mathbf{P}_{\rm c3}:\min_{\tilde{\mathbf{W}}(n)\in\mathcal{M}_{\rm c}}-\sum\nolimits_{k=1}^{K}\frac{\bar{\mu}_k'(n)|\hat{\mathbf{h}}_k^{\rm H}(n)\tilde{\mathbf{W}}(n)\mathbf{E}_k|^2}{\sum_{i=1}^{K}|\hat{\mathbf{h}}_k^{\rm H}(n)\tilde{\mathbf{W}}(n)\mathbf{E}_i|^2+\sigma^2}, \tag{12}$$

where $\hat{\mathbf{h}}_k(n)=\sqrt{p_{\max}}[\mathbf{h}_k(n),0]$ is adjusted to match the problem's dimensionality and scaling. In $\mathcal{M}_{\rm c}$, the objective function (12) is continuous differentiable function from $\mathcal{M}_{\rm c}$ to $\mathbb{R}$. Thus, $\mathbf{P}_{\rm c3}$ can be addressed by MO [8], [12].

2) Solution for $\mathbf{P}_{\rm s}$: As in Section IV-1, $\mathbf{P}_{\rm s}$ is reformulated as a constrained MO problem on manifold $\mathcal{M}_{\rm s}$ as

$$\mathbf{P}_{\rm s1}:\min_{\tilde{\mathbf{V}}(n)\in\mathcal{M}_{\rm s}}f(\tilde{\mathbf{V}}(n))=-\sum_{k=1}^{K}\frac{\hat{\mu}_k(n)|\hat{\mathbf{h}}_k^{\rm H}(n)\tilde{\mathbf{V}}(n)\tilde{\mathbf{E}}_k|^2}{\sum_{i=1}^{K}|\hat{\mathbf{h}}_k^{\rm H}(n)\tilde{\mathbf{V}}(n)\tilde{\mathbf{E}}_i|^2+\sigma^2}, \tag{13a}$$

$$\text{s.t.}\ \ u_l(\tilde{\mathbf{V}}(n))=\Gamma_{\rm th}-\sum\nolimits_{i=1}^{K+1}\hat{\mathbf{g}}_l^{\rm H}(n)\tilde{\mathbf{V}}(n)\tilde{\mathbf{E}}_i\tilde{\mathbf{E}}_i^{\rm H}\tilde{\mathbf{V}}^{\rm H}(n)\hat{\mathbf{g}}_l(n), \tag{13b}$$

where $\hat{\mu}_k(n)=1+\mu_k(n)$ with the optimal $\mu_k^o(n)=\gamma_k(n)$, $\mathcal{M}_{\rm s}=\{\tilde{\mathbf{V}}(n)\in\mathbb{C}^{(M+1)\times(K+1)}\,|\,\mathrm{Tr}(\tilde{\mathbf{V}}(n)\tilde{\mathbf{V}}^{\rm H}(n))=1\}$ is a CSM constructed by normalizing the (6c), where $\tilde{\mathbf{V}}(n)=[\tilde{\mathbf{w}}_1(n),\ldots,\tilde{\mathbf{w}}_K(n),\tilde{\mathbf{s}}(n)]$, $\tilde{\mathbf{w}}_k(n)=[\mathbf{w}_k(n)^{\rm T},\varsigma_k(n)]^{\rm T}$, $\tilde{\mathbf{s}}(n)=[\mathbf{s}(n)^{\rm T},\varsigma_{K+1}(n)]^{\rm T}$, and auxiliary vector $\boldsymbol{\varsigma}(n)=[\varsigma_1(n),\ldots,\varsigma_{K+1}(n)]$ ensures power normalization, i.e., $\mathrm{Tr}(\tilde{\mathbf{V}}(n)\tilde{\mathbf{V}}^{\rm H}(n))=\mathrm{Tr}(\mathbf{V}(n)\mathbf{V}^{\rm H}(n))+\|\boldsymbol{\varsigma}(n)\|_2^2=1$. Note that $\mathbf{P}_{\rm s1}$ is subject to constraint (13b), which extends beyond the manifold constraint. However, (13b) can be incorporated into the objective as a penalty term utilizing ALM [8], [13]. The resulting Lagrangian function is given as [8]

$$\mathcal{L}_\rho(\tilde{\mathbf{V}}(n),\lambda(n))=f(\tilde{\mathbf{V}}(n))+\frac{\rho}{2}\max\left\{0,\frac{\lambda(n)}{\rho}+u_l(\tilde{\mathbf{V}}(n))\right\}^2, \tag{14}$$

Algorithm 1 : ALM-WNI Algorithm

Require: $\mathcal{M}_{\rm s}$, $f(\tilde{\mathbf{V}}(n))$, $u_l(\tilde{\mathbf{V}}(n))$.
Initialization: $\tilde{\mathbf{V}}_0(n) \in \mathcal{M}_{\rm s}$, multiplier $\lambda^0(n) \in \mathbb{R}$, tolerances $\{\epsilon_{\min}, \epsilon_0 > 0, \delta_1 > 0, \delta_2 > 0\}$, penalty ρ_0, reduction factors $\{\theta_\epsilon \in (0,1), \theta_\rho > 1\}$, bounds $\{\lambda^{\min}(n), \lambda^{\max}(n)\} \in \mathbb{R}$, ratio $\tau \in (0,1)$, minimum distance $d_{\min}$, $t = 0$.
while $\text{dist}(f(\tilde{\mathbf{V}}_t(n)), f(\tilde{\mathbf{V}}_{t+1}(n))) \geq \delta_2$ **do**
  Update $\boldsymbol{\eta}_0 = -\text{grad}_{\tilde{\mathbf{V}}_0(n)} \mathcal{L}_\rho(\tilde{\mathbf{V}}(n), \lambda(n))$.
  while $\|\text{grad}_{\tilde{\mathbf{V}}_t} \mathcal{L}_\rho(\tilde{\mathbf{V}}(n), \lambda(n))\|_2 > \delta_1$ **do**
    Compute α_t, update $\tilde{\mathbf{V}}_{t+1}(n)$ via $R_{\tilde{\mathbf{V}}_t(n)}(\alpha_t \boldsymbol{\eta}_t)$, update $\mathcal{T}_{\tilde{\mathbf{V}}_t(n) \to \tilde{\mathbf{V}}_{t+1}(n)}(\boldsymbol{\eta}_t)$, compute β_t, update $\boldsymbol{\eta}_{t+1}$, $t \leftarrow t+1$.
  end while
  Update $\lambda^{t+1}(n)$.
  Set $\sigma_n^{t+1} = \max\left\{\frac{u_l(\tilde{\mathbf{V}}_{t+1}(n))}{\lambda^{t+1}(n)}, -\frac{\lambda^{t+1}(n)}{\rho_t}\right\}$.
  Adjust $\epsilon_{t+1} = \max \epsilon_{\min}, \theta_\epsilon \epsilon_t$.
  $\rho_{t+1} = \begin{cases} \rho_t, & t = 0 \text{ or } \max\limits_n\{|\sigma_n^{t+1}|\} \leq \tau \max\limits_n\{|\sigma_n^t|\}, \\ \theta_\rho \rho_t, & \text{otherwise.} \end{cases}$
  $t \leftarrow t+1$, $\tilde{\mathbf{V}}_t(n) \leftarrow \tilde{\mathbf{V}}_{t+1}(n)$.
end while
Output: $\mathbf{V}^o(n) = \tilde{\mathbf{V}}^o(n)(1:M, K+1)$, $\lambda^o(n)$.

where $\rho > 0$ is a penalty parameter and $\lambda(n)$ is the Lagrange parameter at the n-th subcarrier. The ALM optimizes $\tilde{\mathbf{V}}(n)$ for a given $\lambda(n)$ using the MO, and updates $\lambda(n)$ with a gradient-type rule [14]. Since $\tilde{\mathbf{V}}(n)$ is constrained to $\mathcal{M}_{\rm s}$, $\mathcal{L}_\rho(\tilde{\mathbf{V}}(n), \lambda(n))$ remains differentiable on the manifold, allowing the ALM framework to be applied directly in the Riemannian framework.

Algorithm 1 optimizes $\mathcal{L}_\rho(\tilde{\mathbf{V}}(n), \lambda(n))$ on $\mathcal{M}_{\rm s}$ through four main steps [8], [12]: (i) computing the Riemannian gradient, (ii) determining the search direction and applying the corresponding mapping, (iii) performing retraction, and (iv) updating the Lagrange multipliers. For details of these steps, interested readers are referred to [8], [12], and we omit them for brevity. Moreover, the Euclidean gradient of (14) required for the Riemannian gradient computation is given in (15).

The proposed ALM-WNI algorithm is outlined in Algorithm 1. At each iteration t, it generates a candidate solution that satisfies $\mathcal{L}_\rho(\mathbf{V}_{t+1}(n), \lambda_{t+1}(n)) \leq \mathcal{L}_\rho(\tilde{\mathbf{V}}_t(n), \lambda_t(n)) + \epsilon_t$, where $\{\epsilon_t\}$ is an infinite sequence that converges to zero. This process converges to a Karush-Kuhn-Tucker (KKT) stationary point of $\mathbf{P}_{\rm s1}$ under standard assumptions for the ALM on Riemannian manifolds. The algorithm's objective function is monotonically decreasing, and the upper constraint on it guarantees convergence. With T iterations required for convergence, the overall computational complexity is $\mathcal{O}(T(M(K+1) + M(K+1)^2))$ [8], [12]. In practice, T remains small (typically fewer than five) and does not scale noticeably with M, as reflected in the runtime results. Initialization follows standard practice in MO (e.g., Manopt), where the variables are randomly initialized on the CSM, with $\lambda^0(n) = 1$ [8]. The ALM penalty and multiplier updates mitigate sensitivity to initialization and resolve the trade-off between BG enforcement and SINR maximization by optimizing a single augmented objective on the manifold [8].

Unlike SDR-based CCPA methods using GR [5], [7], **Algorithm 1** enforces sensing constraints directly on $\mathcal{M}_{\rm s}$, ensuring exact constraint satisfaction while maintaining comparable sum-rate performance at lower computational cost [8], [12].

TABLE I: Simulation and algorithm parameters.

Parameter	Value	Parameter	Value
f_c	$54\,\text{GHz}$	$\Gamma_{\rm th}$	$10\,\text{dBm}$
B	$1\,\text{GHz}$	σ^2	$-90\,\text{dBm}$
M	257	$p_{\max}$	$30\,\text{dBm}$
N	8	$\{\delta_1, \delta_2\}$	10^{-6}
K	4	ϵ_0	10^{-3}
L	3	$\{\tau, \theta_\epsilon\}$	0.5
$d_{\min}$	10^{-10}	$\{\rho_0, \theta_\rho\}$	{1, 0.25}
$\epsilon_{\min}$	10^{-6}	$\{\lambda^{\min}(n), \lambda^{\max}(n)\}$	{0, 100}

V. Simulation Results

This section assesses the performance of **Algorithm 1**. The BS is placed at $\{0, 0\}$, while users and targets are randomly distributed within a circular area of radius $50\,\text{m}$. The BS-target sensing directions are set at $-45°$, $30°$, and $70°$. The simulation involves 10^3 Monte Carlo trials. Table I lists the simulation parameters. Per [1], we consider a small fractional bandwidth ($\approx 1.85\,\%$) so frequency-dependent beam-steering effects across subcarriers are limited. However, larger bandwidths can also be investigated by using **Algorithm 1.**

The ALM-WNI is benchmarked against an iterative CCPA [5]. This solves $\mathbf{P}_{\rm c}$ and $\mathbf{P}_{\rm s}$ via SDR and SCA [5]. Specifically, it introduces the lifted variables $\mathbf{W}_k(n) = \mathbf{w}_k(n)\mathbf{w}_k^{\rm H}(n)$ and $\mathbf{S}(n) = \mathbf{s}(n)\mathbf{s}^{\rm H}(n)$, where $\mathbf{W}_k(n)$ and $\mathbf{S}(n)$ are positive semidefinite matrices constrained to be rank one. By dropping the rank-one conditions, $\mathbf{P}_{\rm c}$ and $\mathbf{P}_{\rm s}$ are formed into SDPs [5], which are solved using CVX. A GR procedure is subsequently applied to recover feasible rank-one solutions [7].

The average runtime of ALM-WNI and CCPA is evaluated using MATLAB simulations on an Intel® i7 at $2.50\,\text{GHz}$. For $M = 129$ ALM-WNI and CCPA require approximately $19\,\text{s}$ and $119\,\text{s}$ respectively. When $M = 257$, the runtime increases to $43\,\text{s}$ and $861\,\text{s}$, i.e., a 20-fold reduction. At $M = 321$, the runtimes are $157\,\text{s}$ and $1439\,\text{s}$. Clearly, ALM-WNI scales significantly slowly with M while maintaining comparable or superior C&S performance (Fig. 2, Fig. 3, and Fig. 4).

Figs. 2 and 3 show the transmit BGs of the two algorithms, which exhibit comparable beampatterns. When a subcarrier is assigned to a target, both methods effectively focus power toward that, achieving strong spatial selectivity and improved interference suppression.

Fig. 4 compares the sum rate versus M for both algorithms. As M increases, the sum rate improves for both, reflecting enhanced spatial multiplexing. Notably, ALM-WNI achieves comparable or slightly superior beampattern and sum-rate performance relative to CCPA, while significantly reducing computational complexity.

The improvements in runtime, beampattern, and sum-rate primarily arise from three factors: (i) CCPA operates over the whole space $\mathbb{R}^{MKL}$, whereas ALM-WNI operates on the manifold $\mathcal{M}$ with only $(M+1)(K+L)$ dimensions, yielding a substantial reduction in computational complexity; (ii) ALM-WNI reformulates the non-convex $\mathbf{P}$c and $\mathbf{P}$s directly as a MO framework, avoiding the intermediate approximations required by CCPA. (iii) ALM-WNI jointly optimizes all beamforming vectors through a single variable, which becomes increasingly advantageous in large-scale antenna deployments. In contrast,

$$\nabla_{\tilde{\mathbf{V}}_t(n)}\mathcal{L}_\rho(\tilde{\mathbf{V}}(n),\lambda(n))=\sum_{k=1}^{K}-\hat{\mu}_k(n)\left(\frac{2\hat{\mathbf{h}}_k^{\mathrm{H}}(n)\tilde{\mathbf{V}}_t(n)\tilde{\mathbf{E}}_k\hat{\mathbf{h}}_k(n)\tilde{\mathbf{E}}_k^{\mathrm{H}}}{\sum_{j=1}^{K+1}|\hat{\mathbf{h}}_k^{\mathrm{H}}(n)\tilde{\mathbf{V}}_t(n)\tilde{\mathbf{E}}_j|^2+\sigma^2}-\sum_{i=1}^{K+1}\frac{2|\hat{\mathbf{h}}_k^{\mathrm{H}}(n)\tilde{\mathbf{V}}_t(n)\tilde{\mathbf{E}}_k|^2\hat{\mathbf{h}}_k^{\mathrm{H}}(n)\tilde{\mathbf{V}}_t(n)\tilde{\mathbf{E}}_i\hat{\mathbf{h}}_k(n)\tilde{\mathbf{E}}_i^{\mathrm{H}}}{\left(\sum_{j=1}^{K+1}|\hat{\mathbf{h}}_k^{\mathrm{H}}(n)\tilde{\mathbf{V}}_t(n)\tilde{\mathbf{E}}_j|^2+\sigma^2\right)^2}\right)$$
$$-2\rho\mathbf{1}_{\{\lambda(n)+u_l(\tilde{\mathbf{V}}(n))/\rho\}}\left(\lambda(n)/\rho+u_l(\tilde{\mathbf{V}}(n))\right)\left(\sum_{i=1}^{K+1}\hat{\mathbf{g}}_l^{\mathrm{H}}(n)\tilde{\mathbf{V}}(n)\tilde{\mathbf{E}}_i\hat{\mathbf{g}}_l(n)\tilde{\mathbf{E}}_i^{\mathrm{H}}\right) \quad (15)$$

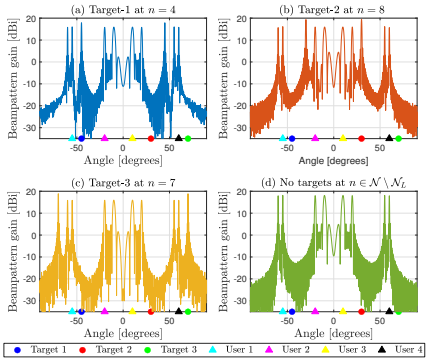

Fig. 2: BGs for the ALM-WNI algorithm with $M = 257$ BS antennas.

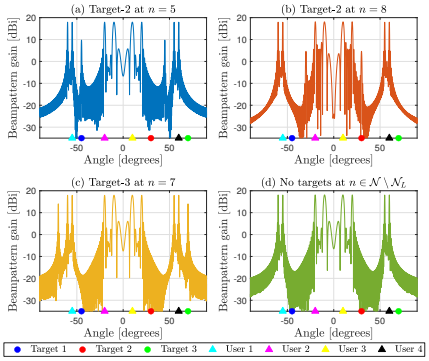

Fig. 3: BGs for the CCPA algorithm with $M = 257$ BS antennas.

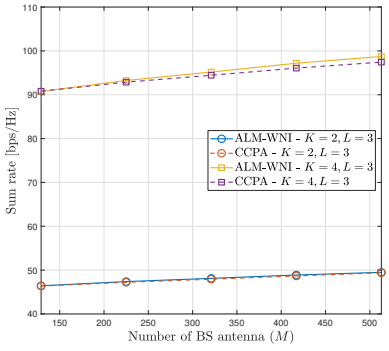

Fig. 4: Sum rate versus the number of BS antennas.

CCPA depends on SCA and SDR, both of which require costly matrix operations whose complexity grows rapidly with M.

VI. Conclusion

This letter introduces ALM-WNI, a low-complexity WB NF-ISAC beamforming algorithm that supports multiple users and targets simultaneously. Subcarriers are allocated and selected for C&S tasks. By exploiting the NF beam-focusing characteristics through location-dependent beamforming that concentrates energy at intended user/target positions, ALM-WNI enhances both C&S performance while suppressing mutual interference between the two tasks. Due to the resulting non-convex problems, the MO approach is employed for CO subcarriers, whereas the ALM-enhanced MO algorithm jointly optimizes communication-sensing subcarriers. Although the problem complexity scales exponentially with the number of antennas, ALM-WNI reduces the search space from MKL dimensions to a lower-dimensional manifold of $(M+1)(K+L)$, yielding substantial computational savings. As a result, it operates significantly faster than the conventional CCPA, making it ideal for large-scale WB NF-ISAC systems.

Future research includes scalable, distributed ALM-WNI for multiple sensing targets, incorporating clutter-aware sensing metrics and user/target mobility, and extending the framework to broader ISAC topologies. Additional opportunities lie in sensitivity and robustness analyses of system parameters and algorithmic hyperparameters, ablation studies of optimization components, advanced SA strategies, and the development of integrated channel-estimation and beam-training strategies tailored for WB NF-ISAC.

References

[1] N. T. Nguyen, N. Shlezinger, Y. C. Eldar, and M. Juntti, "Multiuser MIMO wideband joint communications and sensing system with subcarrier allocation," *IEEE Trans. Signal Process.*, vol. 71, pp. 2997–3013, Sept. 2023.

[2] Z. Wang, X. Mu, and Y. Liu, "Near-field integrated sensing and communications," *IEEE Commun. Lett.*, vol. 27, no. 8, pp. 2048–2052, Aug. 2023.

[3] A. Bazzi *et al.*, "Upper mid-band spectrum for 6G: Vision, opportunity and challenges," *IEEE Commun. Mag.*, vol. 64, no. 1, pp. 206–212, Jan. 2026.

[4] D. Galappaththige, C. Tellambura, and S. Herath, "Wideband cognitive radio for joint communication and sensing: Optimization of subcarrier allocation and beamforming," *IEEE Trans. on Cogn. Commun. Netw.*, vol. 12, pp. 1694–1709, Jan. 2026.

[5] D. Galappaththige, S. Zargari, C. Tellambura, and G. Y. Li, "Near-field ISAC: Beamforming for multi-target detection," *IEEE Wireless Commun. Lett.*, pp. 1–1, Jul. 2024.

[6] ——, "Low-complexity multi-target detection in ELAA ISAC," *IEEE Commun. Lett.*, vol. 29, no. 3, pp. 620–624, Mar. 2025.

[7] S. Boyd and L. Vandenberghe, *Convex Optimization*. Cambridge, U.K.: Cambridge Univ. Press, 2004.

[8] C. Liu and N. Boumal, "Simple algorithms for optimization on Riemannian manifolds with constraints," *Appl. Math. Optim.*, vol. 82, pp. 949–981, Mar. 2020.

[9] Z. He *et al.*, "Full-duplex communication for ISAC: Joint beamforming and power optimization," *IEEE J. Sel. Areas Commun.*, vol. 41, no. 9, pp. 2920–2936, Sept. 2023.

[10] Z. He, W. Xu, H. Shen, Y. Huang, and H. Xiao, "Energy efficient beamforming optimization for integrated sensing and communication," *IEEE Wireless Commun. Lett.*, vol. 11, no. 7, pp. 1374–1378, Jul. 2022.

[11] K. Shen and W. Yu, "Fractional programming for communication systems—part I: Power control and beamforming," *IEEE Trans. Signal Process.*, vol. 66, no. 10, pp. 2616–2630, May 2018.

[12] S. Zargari, D. Galappaththige, C. Tellambura, and H. V. Poor, "A Riemannian manifold approach to constrained resource allocation in ISAC," *IEEE Trans. Commun.*, vol. 73, no. 5, pp. 3655–3670, May 2025.

[13] A. Bazzi and M. Chafii, "On integrated sensing and communication waveforms with tunable PAPR," *IEEE Trans. Wireless Commun.*, vol. 22, no. 11, pp. 7345–7360, Nov. 2023.

[14] E. G. Birgin and J. M. Martínez, *Practical Augmented Lagrangian Methods for Constrained Optimization*. Philadelphia, PA: Soc. Ind. Appl. Math., 2014.